


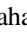







# Characterizing Optical Variability of OJ 287 in 2016–2017

Alok C. Gupta<sup>1,2</sup> , Haritma Gaur<sup>1</sup>, Paul J. Wiita<sup>3</sup> , A. Pandey<sup>1</sup> , P. Kushwaha<sup>4</sup> , S. M. Hu<sup>5</sup>, O. M. Kurtanidze<sup>6,7,8,9</sup> , E. Semkov<sup>10</sup> , G. Damjanovic<sup>11</sup>, A. Goyal<sup>12</sup> , M. Uemura<sup>13</sup>, A. Darriba<sup>14,15</sup>, Xu Chen<sup>5</sup>, O. Vince<sup>11</sup>, M. F. Gu<sup>2</sup>, Z. Zhang<sup>16</sup>, R. Bachev<sup>10</sup>, R. Chanishvili<sup>6</sup>, R. Itoh<sup>17</sup>, M. Kawabata<sup>13</sup>, S. O. Kurtanidze<sup>6</sup>, T. Nakaoka<sup>13</sup>, M. G. Nikolashvili<sup>6</sup>, Ł. Stawarz<sup>12</sup>, and A. Strigachev<sup>10</sup>

<sup>1</sup> Aryabhata Research Institute of Observational Sciences (ARIES), Manora Peak, Nainital—263002, India; [acgupta30@gmail.com](mailto:acgupta30@gmail.com), [harry.gaur31@gmail.com](mailto:harry.gaur31@gmail.com)

<sup>2</sup> Key Laboratory for Research in Galaxies and Cosmology, Shanghai Astronomical Observatory, Chinese Academy of Sciences, Shanghai 200030, People's Republic of China

<sup>3</sup> Department of Physics, The College of New Jersey, 2000 Pennington Road, Ewing, NJ 08628-0718, USA; [wiiatp@tcnj.edu](mailto:wiiatp@tcnj.edu)

<sup>4</sup> Department of Astronomy (IAG-USP), University of Sao Paulo, Sao Paulo 05508-090, Brazil

<sup>5</sup> Shandong Provincial Key Laboratory of Optical Astronomy and Solar-Terrestrial Environment, Institute of Space Sciences, Shandong University, Weihai 264209, People's Republic of China

<sup>6</sup> Abastumani Observatory, Mt. Kanobili, 0301 Abastumani, Georgia

<sup>7</sup> Engelhardt Astronomical Observatory, Kazan Federal University, Tatarstan, Russia

<sup>8</sup> Center for Astrophysics, Guangzhou University, Guangzhou 510006, People's Republic of China

<sup>9</sup> Key Laboratory of Optical Astronomy, National Astronomical Observatories, Chinese Academy of Sciences, Beijing 100012, People's Republic of China

<sup>10</sup> Institute of Astronomy and National Astronomical Observatory, Bulgarian Academy of Sciences, 72 Tsarigradsko Shosse Boulevard, 1784 Sofia, Bulgaria

<sup>11</sup> Astronomical Observatory, Volgina 7, 11060 Belgrade, Serbia

<sup>12</sup> Astronomical Observatory of Jagiellonian University, ul. Orla 171, 30-244 Krakow, Poland

<sup>13</sup> Hiroshima Astrophysical Science Center, Hiroshima University, Kagamiyama 1-3-1, Higashi-Hiroshima 739-8526, Japan

<sup>14</sup> American Association of Variable Star Observers (AAVSO), 49 Bay State Road, Cambridge, MA 02138, USA

<sup>15</sup> Group M1, Centro Astronómico de Avila, Madrid, Spain

<sup>16</sup> Shanghai Astronomical Observatory, Key Laboratory of Radio Astronomy, Chinese Academy of Sciences, Shanghai 200030, People's Republic of China

<sup>17</sup> Department of Physics, Tokyo Institute of Technology, 2-12-1 Ookayama, Meguro-ku, Tokyo 152-8551, Japan

Received 2018 October 3; revised 2018 December 30; accepted 2019 January 12; published 2019 February 5

## Abstract

We report on a recent multiband optical photometric and polarimetric observational campaign of the blazar OJ 287 that was carried out during 2016 September–2017 December. We employed nine telescopes in Bulgaria, China, Georgia, Japan, Serbia, Spain, and the United States. We collected over 1800 photometric image frames in *BVRI* bands and over 100 polarimetric measurements over  $\sim 175$  nights. In 11 nights with many quasi-simultaneous multiband (*V*, *R*, *I*) observations, we did not detect any genuine intraday variability in flux or color. On longer timescales, multiple flaring events were seen. Large changes in color with respect to time and in a color–magnitude diagram were seen, and while only a weak systematic variability trend was noticed in color with respect to time, the color–magnitude diagram shows a bluer-when-brighter trend. Large changes in the degree of polarization and substantial swings in the polarization angle were detected. The fractional Stokes parameters of the polarization showed a systematic trend with time in the beginning of these observations, followed by chaotic changes and then an apparently systematic variation at the end. These polarization changes coincide with the detection and duration of the source at very high energies as seen by VERITAS. The spectral index shows a systematic variation with time and *V*-band magnitude. We briefly discuss possible physical mechanisms that could explain the observed flux, color, polarization, and spectral variability.

**Key words:** BL Lacertae objects: general – BL Lacertae objects: individual (OJ 287) – techniques: photometric – techniques: polarimetric

**Supporting material:** machine-readable tables

## 1. Introduction

Blazars compose a subclass of radio-loud active galactic nuclei in which one of the relativistic jets emanating from the supermassive black hole (SMBH) of mass  $10^6$ – $10^{10} M_{\odot}$  is pointed close to the observer (Woo & Urry 2002). This class is composed of BL Lac objects, which have featureless or very weak emission lines (equivalent widths  $EW \leq 5 \text{ \AA}$ ; Stocke et al. 1991; Marcha et al. 1996), and flat-spectrum radio quasars (FSRQs), which have prominent emission lines (Blandford & Rees 1978; Ghisellini et al. 1997). Blazars show flux variations across the complete electromagnetic (EM) spectrum on all possible timescales, i.e., as short as a few minutes to as long as many years. They show variable polarization in radio to optical bands, and their emission across the EM spectrum is predominantly nonthermal. Their multiwavelength spectral energy distribution (SED) is a double-humped structure in which the low-energy

hump peaks somewhere in IR to soft X-rays and is due to synchrotron emission from nonthermal electrons in the jet, while the high-energy hump peaks in GeV to TeV energies and is probably due to inverse-Compton up-scattering of synchrotron (SSC, synchrotron self-Compton) or external photons (EC, external Compton) by the relativistic electrons producing the synchrotron emission (Kirk et al. 1998; Gaur et al. 2010).

In the age of multiwavelength transient astronomy, blazars are among the best types of persistent, highly variable but noncatastrophic sources for which simultaneous multiwavelength observations should be performed in order to understand their emission mechanism over the complete EM spectrum. Flux and polarization variations in the range of minutes to less than a day are commonly called intraday variability (IDV; Wagner & Witzel 1995) or microvariability (Miller et al. 1989) or intranight variability (Goyal et al. 2012), while those with

timescales from days to a few months are called short-term variability (STV), and timescales of several months to years are known as long-term variability (LTV; Gupta et al. 2004). There is a lengthy series of papers in which blazars' optical flux and polarization variability on diverse timescales are reported (e.g., Andruchow et al. 2003, 2011; Gu et al. 2006; Cellone et al. 2007; Gupta et al. 2008, 2012, 2016, 2017a, 2017b; Gaur et al. 2012c, 2012a, 2012b, 2014, 2015; Larionov et al. 2016; Kushwaha et al. 2018a, and references therein).

The blazar OJ 287 ( $z = 0.306$ ), though identified in 1967 (Dickel et al. 1967), has had data taken in the optical bands since  $\sim 1890$ , and by using about a century-long light curve (LC), Sillanpaa et al. (1988) noticed that it showed double-peaked outbursts almost every 12 yr. To explain them, they proposed a binary black hole model and predicted that the next outbursts would occur in 1994–1995. An extensive optical monitoring campaign known as OJ-94 was organized around the globe, and the predicted double-peaked outbursts were indeed detected in 1994–1995, separated by  $\sim 1.2$  yr (e.g., Sillanpaa et al. 1996a, 1996b). In the next intense observing campaign on OJ 287 during 2005–2007, the double-peaked outbursts were again detected, with the first one at the end of 2005 and the second at the end of 2007, separated by  $\sim 2$  yr (Valtonen et al. 2009). For the most recent prediction of double-peaked outbursts, the first outburst was detected in 2015 December, while the second outburst has yet to be detected (Valtonen et al. 2016; Gupta et al. 2017a) and is predicted for mid-2019 (Valtonen et al. 2016).

The most puzzling issues in the double-peaked outbursts of OJ 287 are the timing of the detection of the second outburst and its strength. From the last three sets of outbursts detected since 1994, it is now clear that they are not exactly periodic. Lehto & Valtonen (1996) analyzed the substructure of major outbursts of OJ 287, identified sharp flares, and connected these with a model in which a secondary SMBH crosses the accretion disk of the primary SMBH during their mutual binary orbit. They estimated the masses of the primary and secondary SMBHs to be  $1.7 \times 10^{10}$  and  $10^8 M_{\odot}$ , respectively. The original model of Sillanpaa et al. (1988) has been modified in different ways over the past decade. Valtonen et al. (2008b) claimed that the changing binary system provides evidence for the loss of orbital energy to within  $\sim 10\%$  of the value predicted by the quadrupole formula for the emission of gravitational waves from the system. However, using 2015 data and considering the higher-order radiation terms, a more recent analysis claimed the loss of orbital energy to be  $\sim 6\%$  less than the quadrupole formula indicates (Dey et al. 2018). Valtonen et al. (2008b, 2010) explain the deviations of the outbursts from strict periodicity as arising from this gravitational-wave-driven inspiraling of the binary black hole system present at the center of OJ 287. According to the latest iteration of the model, the source is an inspiraling and precessing binary SMBH system with a current period of 12.055 yr that decreases by 38 days per century and involves a minimum separation of 1.1 yr between the twin outbursts associated with the disk impacts (Valtonen et al. 2017).

The recent high activity phase of OJ 287 started in 2015 November, around the anticipated time of the latest predicted disk impact optical outburst (Valtonen et al. 2016; Gupta et al. 2017a). The outburst was detected on 2015 December and was the brightest in the past three decades with a relatively low polarization

fraction of  $< 10\%$  (Valtonen et al. 2016; Gupta et al. 2017a; Kushwaha et al. 2018a), as was expected in the binary SMBH model. However, the other key polarization property, the polarization angle (PA), showed an extraordinary  $\sim 200^{\circ}$  systematic change over the duration of the optical flare (Kushwaha et al. 2018a). Similar characteristics (a low degree of polarization (PD), but a strong change in PA), were also seen during the first flare of the 1993–1994 outbursts (Pursimo et al. 2000), while there were not enough observations during the 2005 outburst to know whether this also was the case then (Villforth et al. 2010). This relatively lower polarization compared to that of other flares following it has been argued to be a clear signature of thermal emission (Valtonen et al. 2016). Additionally, a multiwavelength investigation of the near-IR (NIR) to optical SEDs during this duration made in our previous work (Kushwaha et al. 2018a) has, for the first time, reported a bump in the NIR–optical region, consistent with the standard accretion disk impact description of the primary SMBH. Exploration of optical data by Gupta et al. (2017a) found many nights showing IDV during this period.

Using data from the last three outbursts detected since 1994, the masses of the primary and secondary black holes have been estimated to be  $(1.83 \pm 0.01) \times 10^{10} M_{\odot}$  and  $(1.5 \pm 0.1) \times 10^8 M_{\odot}$ , respectively, and the spin of the primary black hole was claimed to be  $0.313 \pm 0.01$  (Valtonen et al. 2016). A strong flare detected in 2016 March was comparably strong to the 2015 December outburst and had a similar polarization (Gupta et al. 2017a; Kushwaha et al. 2018a). In general, blazars, including OJ 287, can evince large-amplitude flares with wide ranges in polarization properties, so determining which of them are those outbursts that are actually caused by the impacts associated with the binary black hole model remains a problem. The binary SMBH model would expect that those particular outbursts are distinguished by a comparatively low optical polarization (Valtonen et al. 2008a).

In the present work, we report detailed optical flux and polarization measurements taken during 2016 September–2017 December of the blazar OJ 287. This is a continuation of an ongoing optical monitoring campaign around the globe of OJ 287 since the year 2015. In that earlier work we detected several flares in flux and significant changes in the PD and PA (Gupta et al. 2017a; Kushwaha et al. 2018a). We will continue our observing campaign on this blazar, at least until we see whether we detect the second predicted outburst of the current pair in 2019.

We structured the paper as follows. In Section 2, we provide information about our new optical photometric and polarimetric observational data and its analysis. In Section 3, we present the results, and we discuss them in Section 4. We summarize our results in Section 5.

## 2. Observations and Data Reductions

Our new optical photometric and polarimetric observational campaigns were carried out from 2016 September to 2017 December. Photometric observations were carried out using seven telescopes located in Japan, China, Bulgaria (two telescopes), Georgia, Serbia, and Spain. Using these seven telescopes, photometric observations were taken on 174 observing nights, during which we collected a total of 1829 image frames of OJ 287 in *B*, *V*, *R*, and *I* optical photometric bands.

We also used the archival optical photometric and polarimetric observations that are performed at Steward Observatory,

**Table 1**

Observation Log of Optical Photometric Observations of the Blazar OJ 287

Date yyyy mm dd	Telescope	Data Points <i>B, V, R, I</i>
2016 Sep 24	A	0, 1, 1, 0
2016 Sep 25	A	0, 1, 1, 0
2016 Oct 09	B	0, 1, 1, 1
2016 Oct 10	B	0, 1, 1, 1

(This table is available in its entirety in machine-readable form.)

University of Arizona, using the 2.3 m Bok and 1.54 m Kuiper telescopes. Polarimetric observations were carried out over 94 observing nights, for which there were a total of 104 polarimetric measurements of OJ 287. We refer to these two telescopes collectively as telescope A in the photometric observation log provided in Table 1. The observations from them are taken from the public archive.<sup>18</sup> These photometric and polarimetric observations of OJ 287 were carried out using the SPOL CCD Imaging/Spectropolarimeter attached to those two telescopes. Details about the instrument, observation, and data analysis are provided in detail in Smith et al. (2009).

Observations from Weihai observatory of Shandong University employed the 1.0 m telescope at Weihai, China. This telescope is named Telescope B in the observation log provided in Table 1. It is a classical Cassegrain telescope with a focal ratio of  $f/8$ . The telescope is equipped with a back-illuminated Andor DZ936 CCD camera and *BVRI* filters. We provide critical information about the telescope and CCD detector in Table 2, and additional details are given in Hu et al. (2014). Sky flats for each filter were taken at twilight, and usually 10 bias frames were taken at the beginning and the end of the observation. All frames were processed automatically by using an Interactive Data Language (IDL) procedure developed locally that is based on the NASA IDL astronomical libraries.<sup>19</sup> First, all frames were bias and flat-field corrected. Second, the magnitude was derived by a differential photometry technique using local standard stars 4, 10, and 11 in the blazar field (Fiorucci & Tosti 1996). The photometry radius was set to 14 pixels, and the inner and outer radii for sky brightness were set to 30 and 40 pixels, respectively. Most of our intensive observations targeting IDV were done using this telescope.

Our optical photometric observing campaign of the blazar OJ 287 in the *B, V, R, and I* passbands continued to use two telescopes in Bulgaria (2.0 m and 50/70 cm Schmidt), which are conflated as Telescope C in Table 1. These telescopes are equipped with CCD detectors and broadband optical filters *B, V, R, and I*. Details of these telescopes and the CCDs mounted on telescope C, as well as details of the reduction procedures used, are given in our earlier papers (Agarwal et al. 2015; Gupta et al. 2016).

Optical *V*-band photometric observations of the blazar OJ 287 were carried out using a Celestron C14 XLT 35.6 cm with reducer  $f/6.3$  located at Las Casqueras, Spain. The telescope is equipped with a CCD camera and *V* broadband optical filter and is called Telescope D in Table 1. Details about this telescope and CCD are given in Table 2. Standard image processing (bias, flat-field, and dark corrections) are applied, and the photometry data were reduced using the Software

MaxIm DL. Reference stars available in the database of the American Association of Variable Star Observers (AAVSO)<sup>20</sup> are used for calibrating the *V* magnitude of OJ 287.

For this campaign, observations of OJ 287 were also carried out using the newly installed 1.4 m telescope at Astronomical Station Vidojevica of the Astronomical Observatory in Belgrade (ASV). The telescope is equipped with a CCD camera and *B, V, R, and I* broadband optical Johnson–Cousins filters. Details are given in Table 2. During our observations, the CCD was cooled to 30°C below ambient. The camera is back-illuminated with high quantum efficiency (QE): peak QE at 550 nm > 90%. The observations carried out by this telescope are given in the observation log reported in Table 1, where it is denoted as Telescope E. Photometric observations were done in  $1 \times 1$  binning mode in *B, V, R, and I* passbands. Standard optical photometric data analysis procedures were adopted (e.g., bias and flat-field correction). To obtain instrumental *B, V, R, and I* magnitudes of OJ 287 and comparison stars, usually we took three image frames per filter, and the result is the average value of the estimated magnitude. Local standard stars in the blazar OJ 287 field are used to calibrate the magnitude of OJ 287 (Fiorucci & Tosti 1996).

Some data from the 70 cm telescope at Abastumani Observatory in Georgia were taken in *R* band, and they are listed as Telescope F in the photometric observation log given in Table 1. The 1.5 m telescope in Kanata, Japan, is named Telescope G in that table, and it also contributed data in *V* and *R* bands on a few nights. Details about Telescopes F and G, their CCDs, their broadband filters, and the data reduction employed are given in our earlier paper (Gupta et al. 2017a).

### 3. Results

In Figure 1 we present the photometric and polarimetric LCs generated from our observing campaign using nine telescopes around the globe during 2016 September–2017 December. We present LCs of the *B, V, R, and I* bands, as well as the PD and PA. The *V*- and *R*-band LCs clearly have the densest observational cadence. The polarimetric observations do not have similarly dense coverage, although the most common photometric observations are made in the *R* band. One can immediately notice that there are several flaring events in the photometric observations in *V* and *R* bands, most of which are also seen in *I*, as well as large changes in the degree of polarization and PA. In the following subsections, we discuss the variability characteristics of the blazar OJ 287 on IDV, STV, and LTV timescales and the nature of the polarization variation.

#### 3.1. LC Analysis Techniques

To quantify the IDV variability results, we use variability detection techniques based on the *F*-test, the so-called  $\chi^2$ -test, and the Levene test, and we describe them briefly in the following subsections. The *F*-test and  $\chi^2$ -test, which are frequently employed in studies of active galactic nucleus variability, assume a normal distribution of the data that is not, in general, true for blazars' LCs. Thus, we have additionally performed the Levene test, which is a nonparametric variance test. We conservatively claim that an LC is variable only if the variability is detected by all three tests. We also calculate the

<sup>18</sup> <http://james.as.arizona.edu/~psmith/Fermi/datause.html>

<sup>19</sup> <http://idlastro.gsfc.nasa.gov/>

<sup>20</sup> <https://www.aavso.org/apps/vsp/>



**Table 2**  
Details of New Telescopes and Instruments

	Weihai, China	Las Casqueras, Spain	ASV, Serbia
Telescope	1.0 m Cassegrain	35.6 cm Schmidt Cassegrain	1.4 m RC Nasmyth
CCD model	Andor DZ936	ATIK 383L+ Monochrome	Apogee Alta U42
Chip size	2048 × 2048 pixels <sup>2</sup>	3354 × 2529 pixels <sup>2</sup>	2048 × 2048 pixels <sup>2</sup>
Scale	0.35 arcsec pixel <sup>-1</sup>	1.38 arcsec pixel <sup>-1</sup>	0.243 arcsec pixel <sup>-1</sup>
Field	12 × 12 arcmin <sup>2</sup>	25.46 × 19.16 arcmin <sup>2</sup>	8.3 × 8.3 arcmin <sup>2</sup>
Gain	1.8 e <sup>-1</sup> ADU <sup>-1</sup>	0.41 e <sup>-1</sup> ADU <sup>-1</sup>	1.25 e <sup>-1</sup> ADU <sup>-1</sup>
Read-out noise	7 e <sup>-1</sup> rms	7 e <sup>-1</sup> rms	7 e <sup>-1</sup> rms
Typical seeing	1.3–2 arcsec	1.5–2.5 arcsec	1–1.5 arcsec

variability amplitude on IDV, STV, and LTV timescales. The method used to determine the variability amplitude is also described briefly below.

### 3.1.1. *F*-test

To quantify any IDV of the blazar OJ 287, we originally adopted the commonly used *F*-test (de Diego 2010) and display these results because many other papers in this field have done so, even though it relies on the data displaying a normal distribution. We employ two comparison stars and so define (Gaur et al. 2012c; Agarwal & Gupta 2015; Gupta et al. 2017a, and the references therein),

$$F_1 = \frac{\text{Var}(\text{BL} - \text{star1})}{\text{Var}(\text{star1} - \text{star2})}, F_2 = \frac{\text{Var}(\text{BL} - \text{star2})}{\text{Var}(\text{star1} - \text{star2})}, \quad (1)$$

where (BL – star 1), (BL – star 2), and (star 1 – star 2) are the differential instrumental magnitudes of blazar and standard star 1, blazar and standard star 2, and standard star 1 and standard star 2, respectively, while Var(BL – star 1), Var(BL – star 2), and Var(star 1 – star 2) are the variances of the differential instrumental magnitudes.

Then, the relevant *F* value is the average of  $F_1$  and  $F_2$ , which is then compared with the critical  $F_{\nu_{bl}, \nu_*}^{(\alpha)}$  value, where  $\alpha$  is the significance level set for the test and  $\nu_{bl}$  and  $\nu_*$  are the number of degrees of freedom, calculated as  $(N - 1)$ , with  $N$  the number of measurements. For IDV detection in the LCs, we have done the *F*-test for  $\alpha$  values of 0.999 and 0.99, which effectively correspond to  $3\sigma$  and  $2.6\sigma$  detections, respectively. The null hypothesis (no variability) is discarded if the *F* value is greater than the critical value, and as usual we claim an LC to be variable if  $F > F_c(0.99)$  (Agarwal & Gupta 2015; Gupta et al. 2017a).

### 3.1.2. $\chi^2$ -test

To quantify the detection of variability of the blazar, we have also used the “so-called”  $\chi^2$ -test (de Diego 2010). This  $\chi^2$  statistic is defined as (e.g., Agarwal & Gupta 2015)

$$\chi^2 = \sum_{i=1}^N \frac{(V_i - \bar{V})^2}{\sigma_i^2}, \quad (2)$$

where  $\bar{V}$  is the average magnitude and  $V_i$  is the magnitude of the  $i$ th observation with a corresponding standard error  $\sigma_i$ . We note that this test assumes a Gaussian scatter and constant mean, neither of which are generally seen in blazar LCs, and so these results are included only because this approach has often been used in other studies. It has been determined that the actual measurement errors are larger than the errors indicated

by photometry software by a factor of 1.3–1.75 (e.g., Gopal-Krishna et al. 2003). Hence, we multiply the errors obtained from the data reductions by a factor of 1.5 (Stalin et al. 2004) to get better estimates of the real photometric errors. The mean value of  $\chi^2$  is then compared with the critical value  $\chi_{\alpha, \nu}^2$ , where  $\alpha$  is the significance level and  $\nu = N - 1$  is the number of degrees of freedom. A value  $\chi^2 > \chi_{\alpha, \nu}^2$  implies the presence of variability.

### 3.1.3. Levene Test

To quantify the IDV in the LCs of the blazar OJ 287, we also have used the nonparametric Levene test (Brown & Forsythe 1974). It compares the variances of different samples and tests the null hypothesis that all the samples are from populations having equal variances. We calculated the statistics  $W_1$  and the null hypothesis probability  $p_1$  for the differential LCs (DLCs) of blazar – Star A and the DLCs of Star A – Star B. Similarly, we found  $W_2$  and  $p_2$  for the DLCs of blazar – Star B and those of Star A – Star B. A  $p$ -value greater than 0.01 indicates that the blazar is nonvariable with respect to the star. The test statistic,  $W$ , is defined as<sup>21</sup>

$$W = \frac{(N - k)}{(k - 1)} \cdot \frac{\sum_{i=1}^k N_i (Z_i - Z_{..})^2}{\sum_{i=1}^k \sum_{j=1}^{N_i} (Z_{ij} - Z_i)^2}, \quad (3)$$

where  $k$  is the number of different groups to which the sampled cases belong,  $N_i$  is the number of cases in the  $i$ th group,  $N$  is the total number of cases in all groups,  $Y_{ij}$  is the value of the measured variable for the  $j$ th case from the  $i$ th group,  $Z_{ij} = |Y_{ij} - \tilde{Y}_i|$ ,  $\tilde{Y}_i$  is a mean of the  $i$ th group,  $|Y_{ij} - \tilde{Y}_i|$ ,  $\tilde{Y}_i$  is a median of the  $i$ th group,  $Z_i = \frac{1}{N_i} \sum_{j=1}^{N_i} Z_{ij}$  is the mean of the  $Z_{ij}$  for group  $i$ ,  $Z_{..} = \frac{1}{N} \sum_{i=1}^k \sum_{j=1}^{N_i} Z_{ij}$  is the mean of all  $Z_{ij}$ .

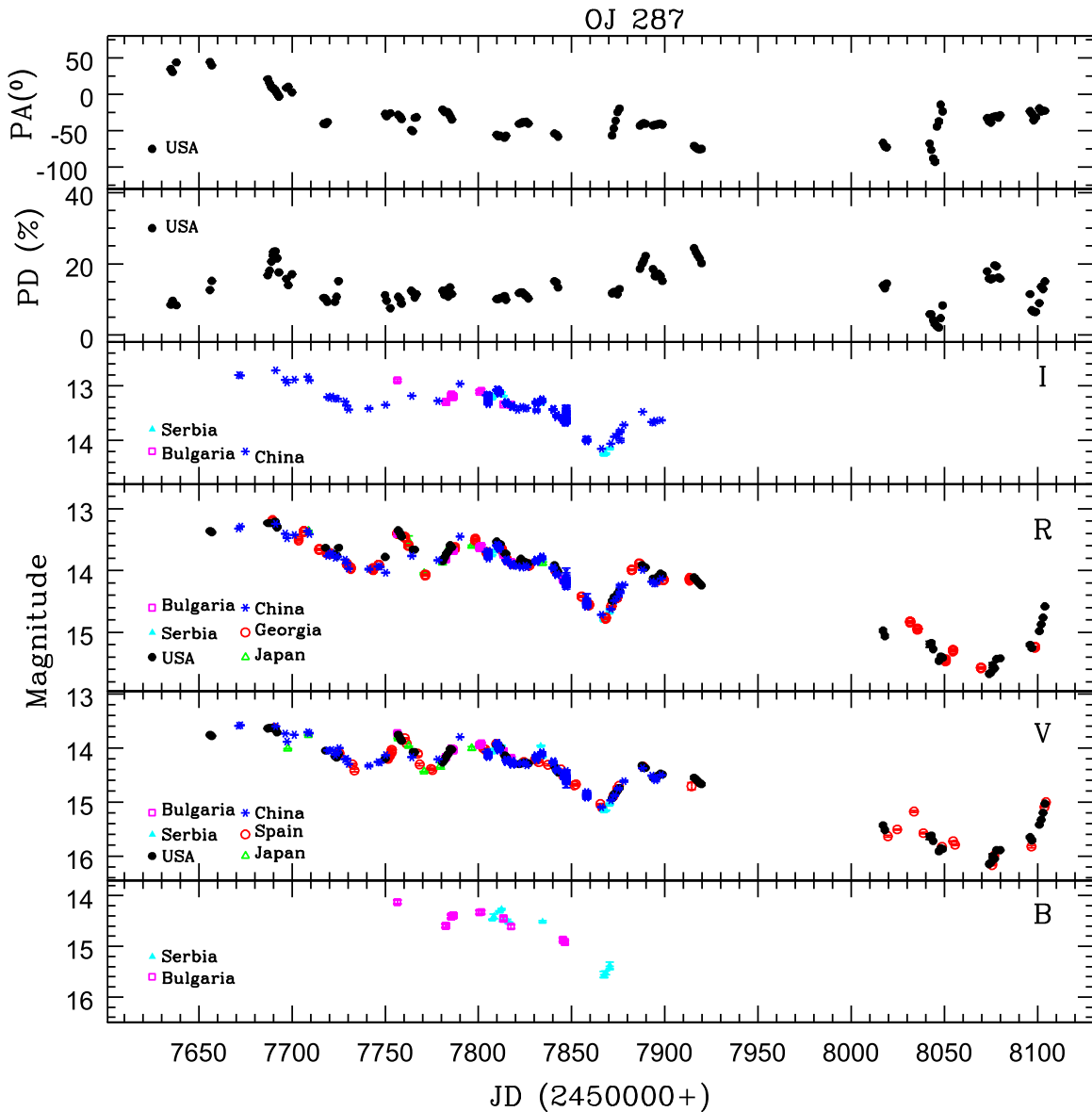
We claimed that the blazar is nonvariable if it is nonvariable with respect to both comparison stars. The values of test statistics and the null hypothesis probabilities are given in Table 3. We list a source as certainly variable (Var) only if it satisfies the criteria of all three tests, i.e., *F*-test,  $\chi^2$ -test, and Levene test.

### 3.1.4. Amplitude of Variability

The percentage of magnitude and color variations on IDV through LTV timescales can be calculated by using the variability amplitude parameter  $A$ , which was introduced by Heidt & Wagner (1996) and defined as

$$A = 100 \times \sqrt{(A_{\max} - A_{\min})^2 - 2\sigma^2} (\%). \quad (4)$$

<sup>21</sup> [https://en.wikipedia.org/wiki/Levene's\\_test](https://en.wikipedia.org/wiki/Levene's_test)



**Figure 1.** Optical flux and polarization variability LCs of OJ 287 during 2015 September–2017 December. From bottom to top, the panels show *B*, *V*, *R*, and *I* calibrated magnitudes, degree of polarization in *R* band, and polarization angle in *R* band, respectively. Different symbols and colors marked inside the panels indicate the data from different telescopes.

Here  $A_{\max}$  and  $A_{\min}$  are the maximum and minimum values in the calibrated magnitude and color of LCs of the blazar, and  $\sigma$  is the average measurement error.

### 3.2. Intraday Flux and Color Variability

Out of  $\sim 175$  observing nights during the campaign, we have many nights when multiple image frames were observed in any specific optical band. But to study the optical flux and color variability properties on IDV timescales, we selected only nights with a minimum of 10 observations in an optical band by a telescope on a particular observing night, and for plotting the IDV LCs, we decided on a minimum of 20 observations in an optical band by a telescope on a particular observing night. Using these criteria, 11 observing nights qualified for IDV flux and color variability analysis, and the results are reported in Table 3, while nine multiband optical IDV flux LCs are plotted in Figure 2.

To investigate the flux and color variability on IDV timescales on the above nights, we have used *F*-test,  $\chi^2$ -test, and Levene test analyses, which were briefly explained in Sections 3.1.1–3.1.3, respectively. Using these tests, the presence or absence of IDV is reported in Table 3, where NV and Var represent nonvariable and variable natures of the LC, respectively. It is clearly seen from the plots in Figure 2, as well as the results reported in Table 3, that, perhaps surprisingly, no genuine IDV was detected in any of the *V*-, *R*-, and *I*-band IDV LCs in the nine nights of intensive observations that were taken during 2017 February 20–2017 April 3. Given the lack of variability in any bands, it is obvious that no color variations were seen on any of these nights on IDV timescales. However, it should be noted that nearly all of these nightly observations were relatively short, spanning between  $\sim 2.5$  and  $\sim 4$  hr, and so the chances of detecting IDV were limited.

From the LCs plotted in Figures 1 and 2, it can be seen that the blazar OJ 287 was in a fairly bright state during much

**Table 3**  
Results of IDV Observations

Date yyyy mm dd	Band	N	F-test $F_1, F_2, F, F_c(0.99), F_c(0.999)$	$\chi^2$ -test		Levene Test		Variable
				$\chi_1^2, \chi_2^2, \chi_{av}^2, \chi_{0.99}^2, \chi_{0.999}^2$		$W_1, p_1$	$W_2, p_2$	
2017 Feb 20	V	74	0.98, 0.67, 0.83, 1.73, 2.08	75.73, 127.15, 101.44, 104.01, 116.09		4.66e-01, 4.96e-01	6.56e-05, 9.94e-01	NV
	R	74	1.50, 0.90, 1.20, 1.73, 2.08	59.06, 70.95, 65.00, 104.01, 116.09		5.29e-01, 4.68e-01	2.88e-01, 5.92e-01	NV
	I	74	1.18, 0.22, 0.70, 1.73, 2.08	320.75, 102.60, 211.67, 104.01, 116.09		5.56e-03, 9.41e-01	1.99e+01, 1.59e-05	NV
	(V - R)	74	1.00, 0.61, 0.81, 1.73, 2.08	75.76, 94.15, 84.96, 104.01, 116.09		6.03e-02, 8.06e-01	1.30e+00, 2.55e-01	NV
	(R - I)	74	1.28, 0.32, 0.80, 1.73, 2.08	209.11, 91.13, 150.12, 104.01, 116.09		5.36e-02, 8.17e-01	1.02e+01, 1.71e-03	NV

**Note.** In the Variable column, Var and NV represent variable and nonvariable, respectively.

(This table is available in its entirety in machine-readable form.)

**Table 4**  
Results of STV and LTV Flux Variations

Band	Duration yyyy mm dd-yyyy mm dd	Variable	A (%)
B	2017 Jan 03-2017 Apr 26	Var	79.5
V	2016 Sep 24-2017 Dec 17	Var	258.2
R	2016 Sep 24-2017 Dec 16	Var	249.1
I	2016 Oct 09-2017 May 24	Var	143.4

**Note.** Var: variable; NV: nonvariable.

**Table 5**  
Color Variation with Respect to Time on Short and Long Timescales

Color Indices	$m_1^a$	$c_1^a$	$r_1^a$	$p_1^a$
R - I	-7.011E-05	1.063	-0.153	2.287E-01
B - V	-1.293E-04	1.377	-0.059	8.296E-01
V - R	2.756E-04	-1.770	0.634	1.029E-14
B - I	2.851E-04	-0.999	0.156	2.888E-01

**Note.**

<sup>a</sup>  $m_1$  = slope and  $c_1$  = intercept of CI against JD;  $r_1$  = Pearson coefficient;  $p_1$  = null hypothesis probability.

of these observations. The brightest state detected in the blazar in the outburst in 2015 December was  $\sim 13.4$  mag in V, 13.0 mag in R, and 12.4 mag in I band (Gupta et al. 2017a). Just from these IDV LCs, we detected OJ 287 in the brightest state on 2017 February 25 when the magnitudes were  $\sim 13.9$  mag in V,  $\sim 13.6$  mag in R, and  $\sim 13.0$  mag in I.

### 3.3. Short-term and Long-term Variability

#### 3.3.1. Flux Variability

Significant flux variability of OJ 287 on STV and LTV timescales is evident from the four lower panels of Figure 1, where the B-, V-, R-, and I-band LCs are shown. We have calculated the variability amplitude in B, V, R, and I optical bands, and these results are reported in Table 4. Observations in the B band were only carried out using telescopes in Bulgaria and Serbia for a total of 16 observing nights between 2017 January 3 and April 3, while we have dense observations carried out in V, R, and I bands. We noticed that the faintest levels of the blazar in B, V, R, and I bands were 14.921 mag at JD 2,457,846.39561, 16.164 mag at JD 2,458,075.58133, 15.670 mag at JD 2,458,073.96976, and

**Table 6**  
Color-Magnitude Dependencies and Color-Magnitude Correlation Coefficients on Short and Long Timescales

Color Indices	$m_2^a$	$c_2^a$	$r_2^a$	$p_2^a$
R - I	7.447E-02	-0.513	0.487	3.319E-08
B - V	2.446E-02	0.022	0.097	0.721
V - R	4.093E-02	-0.209	0.440	1.577E-09
B - I	9.934E-02	-0.174	0.477	0.061

**Note.**

<sup>a</sup>  $m_2$  = slope and  $c_2$  = intercept of CI against V;  $r_2$  = Pearson coefficient;  $p_2$  = null hypothesis probability.

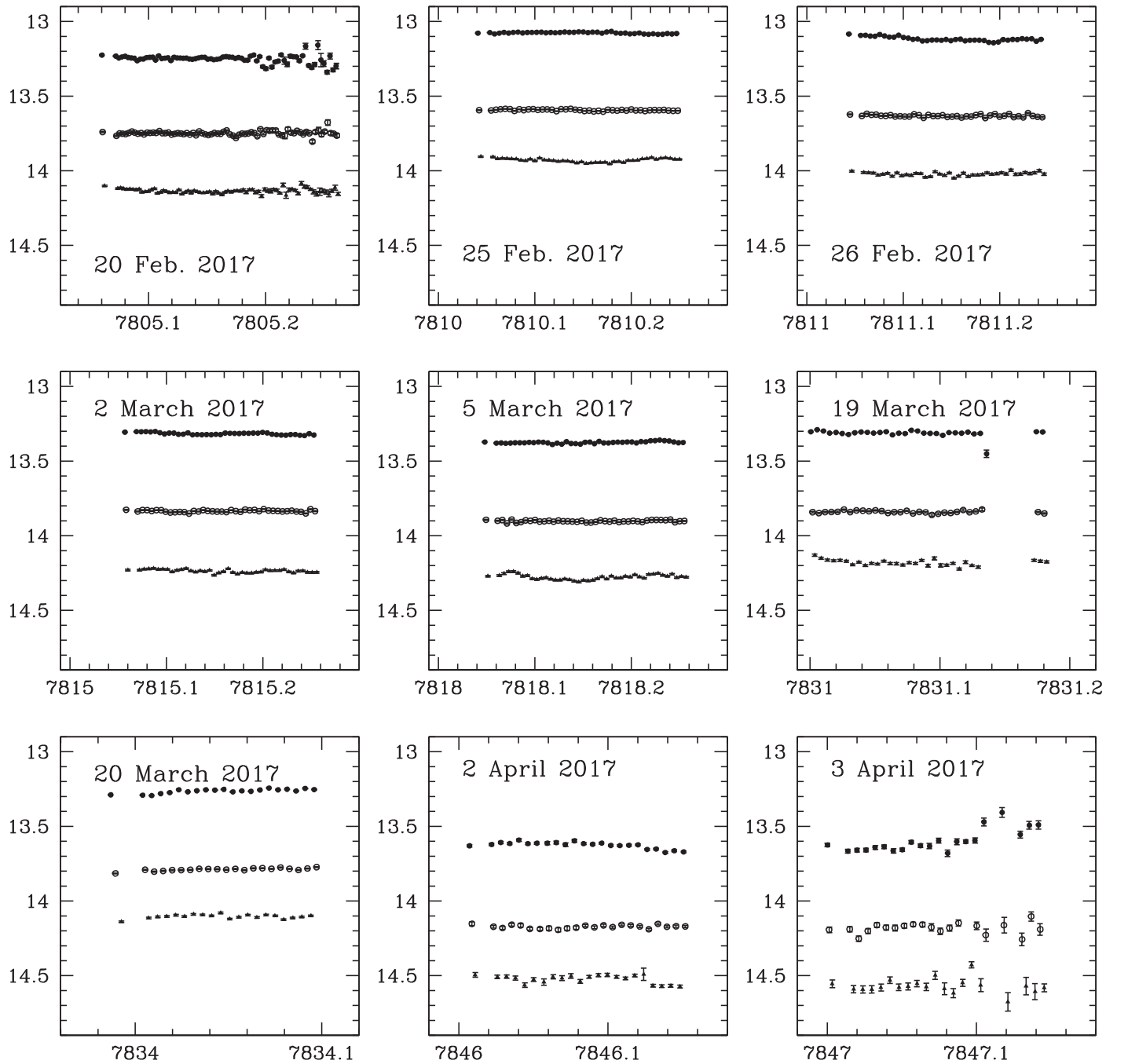
14.154 mag at JD 2,457,866.00547, respectively. Similarly, the brightest levels we observed of the blazar in the B, V, R, and I bands were 14.126 mag at JD 2,457,756.53125, 13.582 mag at JD 2,457,672.36782, 13.179 mag at JD 2,457,679.620, and 12.720 mag at JD 2,457,691.29261, respectively. The amplitudes of variation in B, V, R, and I bands are 79.5%, 258.2%, 249.1%, and 143.4%, respectively, but the smaller values for the B and I bands are explained by the relative paucity of data for them, as all colors are seen to vary together when data were taken for all of them. It can be seen from Figure 1 that small flares are superimposed on a long-term trend. The implications of these results are discussed in Section 4.

#### 3.3.2. Color Variability

Optical color variations with respect to time (color vs. time) and with respect to V-band magnitude (color versus magnitude) are plotted in Figures 3 and 4, respectively. On visual inspection both figures show clear color variations. However, it seems that there are no consistent systematic trends in the color variations, as shown by straight line fits to the color versus time plot in Figure 3. However, the color versus magnitude plots in Figure 4 show bluer-when-brighter (BWB) trends, which are significant for the more frequently measured V - R and R - I colors. Here lines,  $Y = mX + c$ , are fitted in to each panel in Figures 3 and 4. The values of the slopes,  $m$ , the intercepts,  $c$ , the linear Pearson correlation coefficients,  $r$ , and the corresponding null hypothesis probability,  $p$ , results for color versus time and color versus magnitude are reported in Tables 5 and 6, respectively.

#### 3.3.3. Polarization Variability

In Figure 1 we plotted optical magnitudes of OJ 287, as well as degree of polarization and PA. It is clear from visual

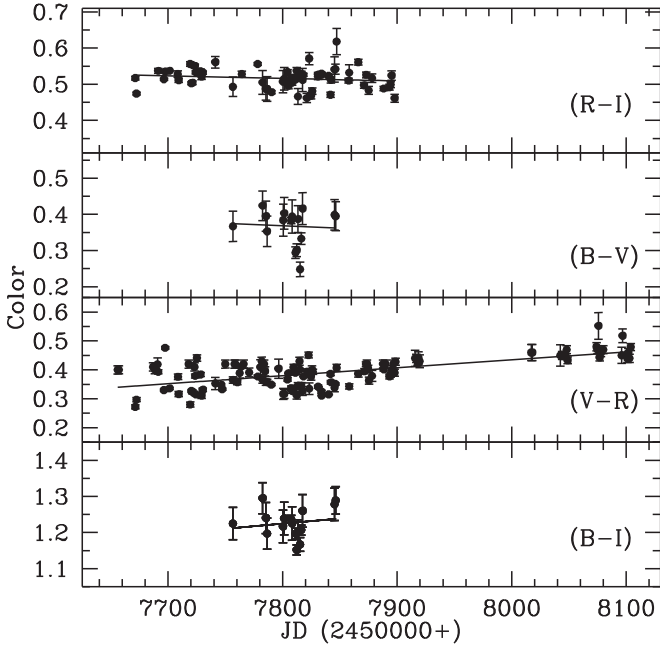


**Figure 2.** Intraday LCs for OJ 287 in  $V$ ,  $R$ , and  $I$  filters. Filled triangles, open circles, and filled circles represent data in  $V$ ,  $R$ , and  $I$  filters, respectively. The  $X$ -axis is JD (2,450,000+), and the  $Y$ -axis is the magnitude in each plot, where observation dates are indicated in each plot.

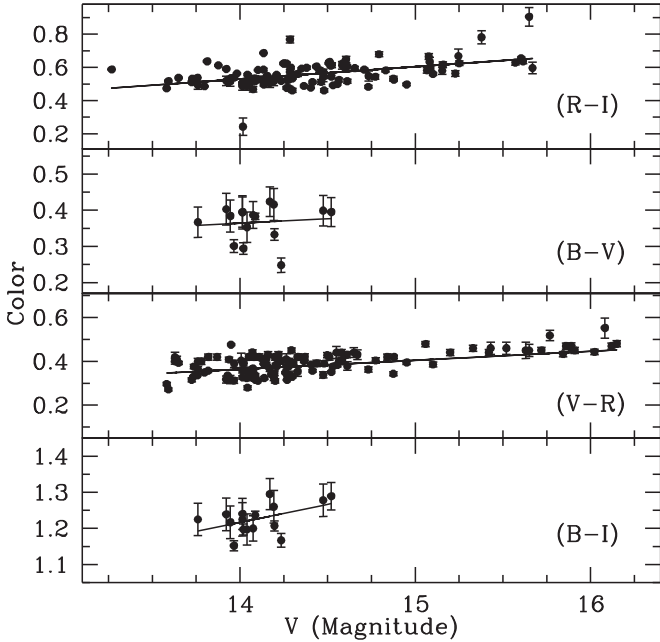
inspection of the figure that the source exhibited large variations in PD and PA, as well as overall flux. We noticed the following combinations of variation of flux, degree of polarization, and PA: (i) at  $\sim$ JD 2,457,682 the flare peak at  $R = 12.957$  mag corresponds to a PD of 20%, and  $PA = 15^\circ$ ; (ii) at  $\sim$ JD 2,457,755 the flare peak at  $R = 13.35$  is anticorrelated with PD at only 9%, and  $PA = -35^\circ$ ; (iii) at  $\sim$ JD 2,457,790 the flare peak at  $R = 13.437$  mag corresponds to PD = 13%, and  $PA = -63^\circ$ ; (iv) the lowest flux state at  $\sim$ JD 2,458,074, with  $R = 15.670$  mag, is anticorrelated, having a high PD  $\sim$  20%, and  $PA = -25^\circ$ .

Figure 5 presents the polarization in terms of the normalized Stokes parameters,  $Q/I$  versus  $U/I$ , for these data. Here we

have used the data taken during JD 2,457,633 to 2,457,920, before the  $\sim$ 100-day gap when the blazar could not be observed from the ground. The more limited polarimetric observations taken afterward have not been used in the analysis. We note that there appears to be a systematic change in the polarization fluxes with the PA during the first  $\sim$ 100 days that evinces a clockwise loop-like structure (shown by black to purple points). During the middle part of the observations (red to orange points), there is relatively less change in the Stokes parameters with roughly random variations. However, there is a hint of the beginning of a systematic change over the last 50 days of the observations (yellow points). Over all, the intensity variations in the



**Figure 3.** Optical color variability LCs covering the entire monitoring period of OJ 287.

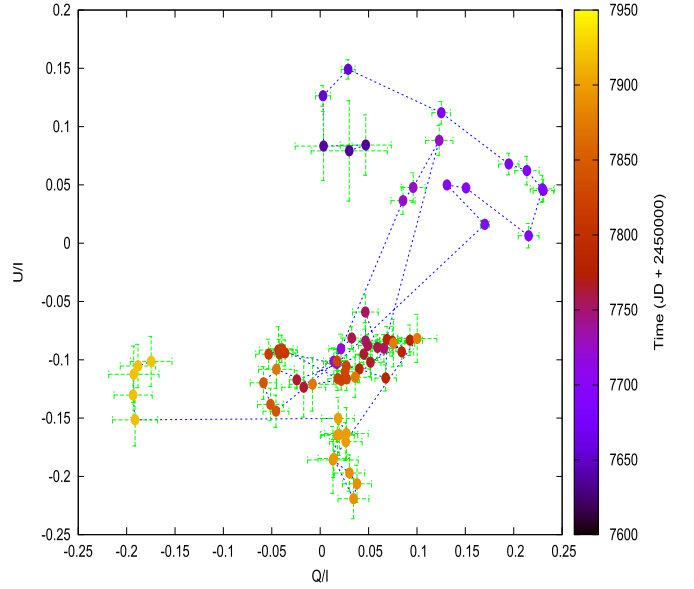


**Figure 4.** Optical color-magnitude plots of OJ 287 during our entire monitoring period.

$(Q, U)$ -plane are mostly reminiscent of a random walk, indicating that emission is resulting from different regions with different magnetic field orientations (Moore et al. 1982), throughout the course of observations presented in this study.

### 3.3.4. Spectral Index Variation and SED

We have dense sampling in  $V$  and  $R$  bands during our whole observing campaign, so we also calculated spectral indices for all the epochs where we have  $V$ - and  $R$ -band data on the same



**Figure 5.** Fractional polarization variations over the course of data presented in this study.

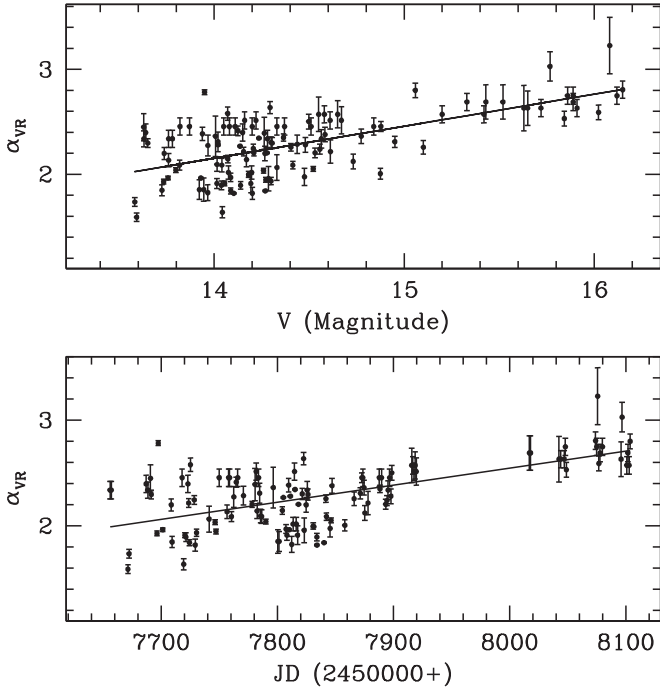
JD, following Wiercholska et al. (2015),

$$\alpha_{VR} = \frac{0.4(V - R)}{\log(\nu_V / \nu_R)}, \quad (5)$$

where  $\nu_V$  and  $\nu_R$  are effective frequencies of  $V$  and  $R$  bands, respectively (Bessell et al. 1998). It should be noted that spectral index estimated using this expression differs from the usual index (in  $F_\nu \propto \nu^{-\alpha}$ ) by a constant factor related to the zero-point magnitude of the two bands. The spectral indices with respect to time and with respect to  $V$ -band magnitude are plotted in the bottom and top panels of Figure 6, respectively. It is clearly seen that there are large variations in  $\alpha_{VR}$  between  $\sim 1.5$  and  $\sim 3.2$ . From the bottom panel of Figure 6 it is clear that the spectral index systematically increased with respect to time, and from the top panel of Figure 6, the spectral index increases with respect to increasing  $V$ -band magnitude, confirming the BWB result. The straight line fitting parameters are given in Table 7.

To further explore the systematic change of the spectral index with time, as well as magnitude, as seen in Figure 6, we have generated optical SEDs during different optical flux states of the source. We have taken quasi-simultaneous  $B$ -,  $V$ -,  $R$ -, and  $I$ -band data points at four different states to produce optical SEDs. These states are as follows: during outburst 1 from JD 2,457,756.5 to 2,457,757.5, during outburst 2 from JD 2,457,811.2 to 2,457,812.5, an intermediate state from JD 2,457,844.5 to 2,457,845.5, and a low state from JD 2,457,867.5 to 2,457,868.5. Unfortunately, we only have data in two bands ( $V$  and  $R$ ) at the lowest flux state of the source on JD 2,458,074 during this observing campaign and so could not plot an optical SED for it. To generate the SEDs, calibrated magnitudes of OJ 287 in  $B$ ,  $V$ ,  $R$ , and  $I$  bands are adjusted for Galactic absorption, with  $A_B = 0.102$  mag,  $A_V = 0.075$  mag,  $A_R = 0.063$  mag, and  $A_I = 0.045$  mag, respectively (Cardelli et al. 1989; Bessell et al. 1998). The SEDs of these four different flux states of the source are plotted in Figure 7. During the observing campaign, there were other periods of strong flaring, as well as intermediate or low flux states of the





**Figure 6.** Optical spectral index variation with respect to time and  $V$ -band magnitude covering the entire monitoring period of OJ 287.

**Table 7**

Spectral Index Variation with Respect to JD and  $V$ -band Magnitude for the Entire Period of the Observation Campaign of OJ 287

Parameter	$m_3^a$	$c_3^a$	$r_3^a$	$p_3^a$
$\alpha_{VR}$ versus JD	1.612E-03	-10.350	0.634	1.013E-14
$\alpha_{VR}$ versus $V$ (mag)	3.054E-01	- 2.123	0.650	1.235E-15

**Note.**

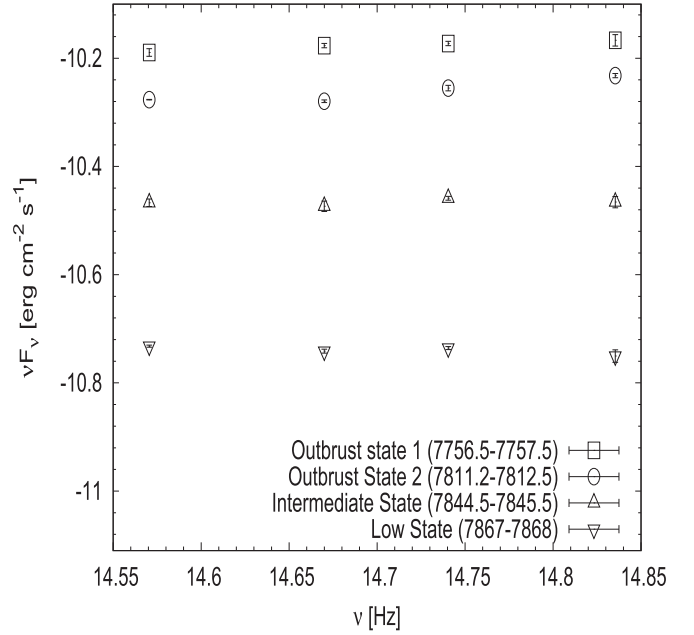
<sup>a</sup>  $m_3$  = slope and  $c_3$  = intercept of  $\alpha$  against JD or  $V$ ;  $r_3$  = Pearson coefficient;  $p_3$  = null hypothesis probability.

source, but unfortunately we do not have quasi-simultaneous (within a day) observations in at least three optical bands, so those are not considered for making SEDs.

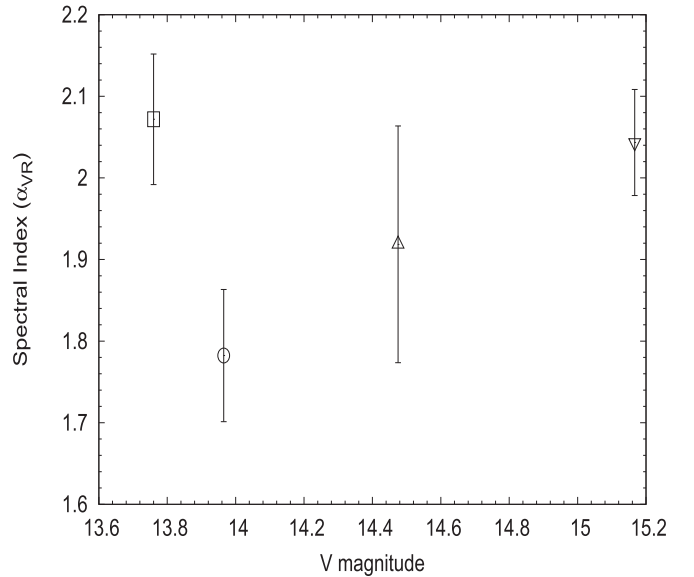
The most striking observation about the optical SEDs during the current period is their relative flatness in the intermediate and low states, while there is a slightly rising trend with frequency during outbursts 1 and 2. These are very different compared to the previous optical SEDs of the source so far, which showed a clear declining trend at higher frequencies (Kushwaha et al. 2013, 2018a; Gupta et al. 2017a). The corresponding spectral indices for the four SEDs with respect to  $V$ -band magnitude, following Equation (4), are shown in Figure 8. The indices clearly reflect the variation between the two bands, with indices being lower for harder spectra, as can be seen clearly in the SEDs for the respective states.

#### 4. Discussion

OJ 287 is currently in an enhanced activity phase that started in 2015 November (Gupta et al. 2017a; Kushwaha et al. 2018a, 2018b). The timing of the beginning of this optical enhancement was in accordance with the inspiraling binary SMBH model (Valtonen et al. 2016, and references therein), which attributes the  $\sim 12$  yr quasi-periodicity seen in the optical



**Figure 7.** Optical SED of OJ 287 at different flux states.



**Figure 8.** Variation of optical spectral index of OJ 287 with  $V$  magnitude during two outburst states, an intermediate state, and a low state, where the symbols have the same meaning as in Figure 7.

data to the impact of the secondary SMBH on the accretion disk of the primary. Apart from confirming the model predictions, studies and observations of OJ 287 since then have resulted in reporting of many new features in the spectral, temporal, and polarization domains. These include a possible thermal bump in the NIR–optical region consistent with primary SMBH accretion disk emission (Kushwaha et al. 2018a), a change in shape of  $\gamma$ -ray SEDs and shifts in its peak position (Kushwaha et al. 2018a, 2018b), and the first ever detection at very high energies (VHEs,  $E > 100$  GeV; O’Brien 2017). The work presented here is part of ongoing efforts to explore the source activity and features between the two claimed disk impacts via dense follow-up at optical energies. A significant part of the present data has already been presented in another work focusing on multiwavelength aspects

of the source (Kushwaha et al. 2018b), but that paper was concerned with timescales of interest associated with the multiwavelength data cadence. Here, we are focused on investigation on diverse timescales from IDV to LTV that are allowed by the current data, which was not possible with the multiwavelength data owing to either the low cadence of X-ray and  $\gamma$ -ray data or the lack of good photon statistics for the latter on all the timescales of the optical data considered here.

The data presented here correspond to the 2016 September–2017 December period, when we have obtained extensive optical photometric and polarimetric monitoring of OJ 287 on a total of  $\sim 175$  nights from seven different optical telescopes around the globe. Archival data from Steward Observatory are also included in our studies. We have searched for flux and color variations on IDV, STV, and LTV timescales. We have also searched for color variations with respect to time, color dependence on magnitude, spectral index variation, SED changes, and polarization variations on LTV timescales. Investigation of IDV on 11 nights when we have quasi-simultaneous multiband ( $V$ ,  $R$ ,  $I$ ) observations showed no significant IDV in fluxes or colors (Table 3). On the other hand, on STV and LTV timescales the LCs show strong evidence of major flux changes, with amplitude variations reaching  $\sim 250\%$  (Table 4), including multiple instances of flaring. The lower detected variabilities for the  $B$  and  $I$  bands are almost certainly due to the lesser amounts of data for them. There is some evolution of the best-measured ( $V-R$ ) color with time (Table 5, Figure 3), but there are clear systematic variations of color with respect to the  $V$ -band measurements (Table 6, Figure 4), referred to generally as a BWB trend, which is a result of a new nonthermal high-frequency-peaked blazar (HBL) component (Kushwaha et al. 2018b).

In the polarization domain, the source reflects the activity seen in the flux variations on similar timescales. Broadly, most of the flux increments are accompanied by an increase in PD, which is also associated with frequent changes in the PA by amounts of  $\lesssim 50^\circ$ . The Stokes parameters show a systematic clockwise trend during the first 100 days, followed by an erratic variation and finally a return to a systematic trend toward the end (Figure 5), indicating the importance of magnetic field changes. We note that the transition from the clockwise trend to the erratic one coincided with the VHE detection and the return to a trend occurred when the source was no longer detectable at those energies (O’Brien 2017). It should be further noted that PA (after correcting for the  $\pm 180^\circ$  ambiguity) shows a smooth systematic change of  $\sim 125^\circ$ – $150^\circ$  with small-amplitude variations superimposed on it.

The trends and variations seen in the temporal and polarization domains are also reflected in the spectral domain where the VR spectral index shows a systematic change with both  $V$ -band magnitude and time (Figure 6). This similar trend with both  $V$ -band measurement and flux is reflective of a systematic decline of emission level with time, as can be seen in the LCs. Interestingly, the declining trend is similar to the systematic trend of change in the PA. Further, the flat or uprising optical SEDs suggest that this trend is due to broadband emission. Though there is strong variability with some systematic trends, the variations during the current phase are very different from those seen during our previous observation campaign (Gupta et al. 2017a). Most interestingly, the current data do not display IDV variability despite similar large-amplitude variations on LTV and STV timescales,

thereby suggesting that the observed variability is governed by regions of larger sizes corresponding to the LTV/STV timescales.

Blazar flux variability on IDV timescales is the most puzzling, and during low states it may allow us to probe very close to the central SMBH. IDV in high flux states can be due to evolution of the electron energy density distribution of the relativistic charged particles in which shocks will accelerate relativistic particles in turbulent regions of plasma jets that then cool and lead to a variable synchrotron emission (Marscher et al. 1992; Marscher 2014; Calafut & Wiita 2015; O’Riordan et al. 2017). The most extreme IDV might require acceleration of small regions within the jets to extremely high Lorentz factors (e.g., Giannios et al. 2009). Optical flux variability detected on IDV timescales in low states can be explained by models based on the accretion disk (e.g., Chakrabarti & Wiita 1993; Mangalam & Wiita 1993). Our lack of detection of genuine IDV in any of the 11 densely sampled nights for OJ 287 indicates that during this period the jet emission was quite uniform and that relativistic shock directions did not quickly change with respect to our line of sight. Here we can safely rule out accretion-disk-based models because the source was observed in an overall high flux state, when jet emission must dominate and no flux or color variations were noticed on IDV timescales.

Blazar emission on STV and LTV timescales is dominated by nonthermal jet emission throughout the EM spectrum and can also explain the optical flux and polarization variability on diverse timescales. Shock-in-jet models (e.g., Hughes et al. 1985; Marscher & Gear 1985; Spada et al. 2001; Graff et al. 2008; Joshi & Böttcher 2011, and references therein) can explain the general behavior of flux variability on diverse timescales, while the polarization variability also can be explained by these models (e.g., Marscher et al. 2008; Larionov et al. 2013, and references therein), particularly when supplemented with turbulence (Marscher 2014). Changes in the physical parameters set up close to the base of the jet, including velocity, electron density, magnetic field, etc., can produce a new shock that can lead to a flaring event when moving along the inhomogeneous relativistic jet. Geometrical effects from jet bending, precession, or internal helical structures can lead to changes in the Doppler boosting of the jet emission, which can produce a wide variety of flux variations on STV and LTV timescales in blazars (e.g., Camenzind & Krockenberger 1992; Gopal-Krishna & Wiita 1992; Pollack et al. 2016).

The four optical SEDs (Figure 7) during different flux states are almost flat, except for changes in the overall level of emission. In fact, they suggest more emission at the high-frequency end, which is very different compared to previous SEDs (Kushwaha et al. 2013, 2018a; Gupta et al. 2017a, and references therein), where normally declining emission is seen. Since any thermal features are not expected to vary appreciably on timescales of days or months, the flatness of the SED and the blue bump emission possibly seen in our previous work (Gupta et al. 2017a; see also Kushwaha et al. 2018a) suggest a contribution from another component in the optical that makes the emission increase at high frequencies (e.g., Kushwaha et al. 2018b). This is clear from the investigation of the broadband SED by Kushwaha et al. (2018b), with OJ 287 SEDs being a sum of a low-frequency-peaked blazar, which is the typical SED of OJ 287, and a new HBL spectral component during the

high activity states. This new component, peaking in the UV–X-ray region, is responsible for the relative flatness of the SEDs. This is also consistent with the high PD, and strong changes of it during these observations, often associated with PA swings, and the systematic variation in the fractional polarization suggest the second component to be nonthermal in nature, as also reflected in the strong variability of the optical  $V - R$  spectral index on daily timescales (Figure 6). Although OJ 287 is fundamentally a BL Lac object and has at most very weak emission lines, they may be present at the level of  $\sim 10^{42}$ – $10^{43}$  erg s $^{-1}$  and were apparently seen during the interaction time suggested by the binary SMBH model (Nilsson et al. 2010), and they also might be relevant for explaining the overall multiwavelength SED shift in the  $\gamma$ -ray peak (Gupta et al. 2017a; Kushwaha et al. 2018a).

In our flux and polarization monitoring campaign of OJ 287 during 2016–2017, we noticed interesting relations between the fluxes, degree of polarization, and PA. There is a systematic swing of  $\sim 150^\circ$  in PA from  $\sim$ JD 2,457,630 to JD 2,457,850, with a few superimposed short-term fluctuations of up to  $\sim 50^\circ$ . But during this period the degree of polarization has large variations, from a few percent to over 20%. These changes in flux, PD, and PA are quite complex. Interestingly, the fractional polarization shows a systematic clockwise variation during the first 100 days, followed by an essentially random trend and again returning to systematic variation toward the end. It should be noted that the lack of observations before MJD  $\sim 57,650$  allow an ambiguity of  $\pm 180^\circ$  in representation of PA. In our presentation of the PA changes here we chose a smooth variation over a big jump, and so it differs by  $180^\circ$  from the presentation of some similar data by Valtonen et al. (2017). The choice is based on the fact that the PD variation seen here is almost always associated with PA change and the fact that the fractional polarization shows both systematic and chaotic trends. Further, in random variation models, a sudden jump of no more than  $\pm 90^\circ$  is expected (e.g., Marscher 2014).

In the basic shock-in-jet model, where the shocked region strengthens the ordering of the magnetic field, one can expect a positive correlation between flux and polarization, i.e., an increase in polarization with an increase in flux (Marscher & Gear 1985; Marscher 1996; Hagen-Thorn et al. 2008). There are several cases in which blazar flux and degree of polarization show such positive correlations (e.g., Larionov et al. 2008, 2013, 2016, and references therein). Detection of anticorrelated flux and degree of polarization is rare but has been occasionally noticed before (e.g., Gaur et al. 2014). During this observing campaign, we noticed that when the source goes into the lowest flux state, at  $\sim$ JD 2,457,865, the PD is rather high and there is evidence of large swings of  $\sim 70^\circ$  of the PA. Marscher et al. (2008) gave a generalized model for variation in optical flux, degree of polarization, and PA. The model involves a shock wave leaving the close vicinity of the central SMBH and propagating down only a portion of the jet’s cross section, which leads to the disturbance following a spiral path in a jet that is accelerating and becoming more collimated. Larionov et al. (2013) extended the work of Marscher et al. (2008) and applied this generalized model to multiwavelength variations of an outburst detected in the blazar S5 0716+714. In the model of Larionov et al. (2013), if one changes the bulk Lorentz factor  $\Gamma$ , even if the remaining parameters (e.g., jet viewing angle, temporal evolution of the outburst, shocked plasma compression ratio  $k$ , spectral index  $\alpha$ , and pitch angle of the spiral

motion) are kept constant, different combinations in the variations in flux, polarization, and PA can be observed.

## 5. Summary

We summarize below our results:

1. The blazar OJ 287 was in a fairly bright state between 2016 September and 2017 December, and several large and small flares were observed in optical bands.
2. Using our selection criteria, we had 11 nights during which multiband intraday LCs could be extracted, but we never saw fast (IDV) variations in flux or color.
3. On longer STV and LTV timescales OJ 287 showed large-amplitude flux variation in all  $B$ ,  $V$ ,  $R$ , and  $I$  bands with variability in respective band similar to what was found in the previous study (Gupta et al. 2017a).
4. Color variations are noticed on STV and LTV timescales in both color versus time and color versus magnitude plots. A BWB trend is noticed between the best-sampled  $V$  and  $R$  bands.
5. There are strong variations in degree of polarization and large swings in PA. For most of the time, both flux and polarization show complex variations.
6. On two occasions around JD 2,457,755 and JD 2,458,074, we noticed that there are strong evidences of anticorrelation in flux with degree of polarization and PA.
7. Through plotting the Stokes parameters, we observed that the fractional polarization exhibited a systematic clockwise trend with time during the first 100 days, followed by a more restricted and essentially random variation, and then it appears to revert to a systematic variation. This duration and trend are coincident with the source’s VHE activity (O’Brien 2017), suggesting a role magnetic field for that activity.

Data from the Steward Observatory spectropolarimetric monitoring project were used. This program is supported by Fermi Guest Investigator grants NNX08AW56G, NNX09AU10G, NNX12AO93G, and NNX15AU81G.

We thank the anonymous referees for useful comments. The work of A.C.G. and A.P. is partially supported by Indo-Poland project no. DST/INT/POL/P19/2016 funded by the Department of Science and Technology (DST), Government of India. A.C.G.’s work is also partially supported by Chinese Academy of Sciences (CAS) President’s International Fellowship Initiative (PIFI) grant no. 2016VMB073. H.G. acknowledges financial support from the Department of Science & Technology, India, through INSPIRE faculty award IFA17-PH197 at ARIES, Nainital. P.J.W. is grateful for hospitality at KIPAC, Stanford University, and SHAO during a sabbatical. P.K. acknowledges support from FAPESP grant no. 2015/13933-0. The Abastumani team acknowledges financial support by the Shota Rustaveli National Science Foundation under contract FR/217554/16. O.M.K. acknowledges China NSF grants NSFC11733001 and NSFCU1531245. S.M.H.’s work is supported by the National Natural Science Foundation of China under grant no. 11873035, Natural Science Foundation of Shandong province (no. JQ201702), and also partly supported by the Young Scholars Program of Shandong University, Weihai (no. 20820162003). The work of E.S., A.S., and R.B. was partially supported by the Bulgarian National Science Fund of the Ministry of Education and



Science under the grants DN 08-1/2016 and DN 18-13/2017. G.D. and O.V. gratefully acknowledge the observing grant support from the Institute of Astronomy and NAO Rozhen, BAS, via bilateral joint research project “Study of ICRF radio-sources and fast variable astronomical objects” (the head is G.D.). This work is a part of project no. 176011 “Dynamics and kinematics of celestial bodies and systems,” no. 176004 “Stellar physics,” and no. 176021 “Visible and invisible matter in nearby galaxies: theory and observations” supported by the Ministry of Education, Science and Technological Development of the Republic of Serbia. A.G. acknowledges full support from the Polish National Science Centre (NCN) through the grant 2012/04/A/ST9/00083 and partial support from the UMO-2016/22/E/ST9/00061. Ł.S. is supported by Polish NSC grant UMO-2016/22/E/ST9/00061. M.F.G. is supported by the National Science Foundation of China (grants 11473054 and U1531245). Z.Z. is thankful for support from the CAS Hundred-Talented program (Y787081009).

### ORCID iDs

Alok C. Gupta  <https://orcid.org/0000-0002-9331-4388>  
 Paul J. Wiita  <https://orcid.org/0000-0002-1029-3746>  
 A. Pandey  <https://orcid.org/0000-0003-3820-0887>  
 P. Kushwaha  <https://orcid.org/0000-0001-6890-2236>  
 O. M. Kurtanidze  <https://orcid.org/0000-0001-5385-0576>  
 E. Semkov  <https://orcid.org/0000-0002-1839-3936>  
 A. Goyal  <https://orcid.org/0000-0002-2224-6664>

### References

- Agarwal, A., & Gupta, A. C. 2015, *MNRAS*, **450**, 541  
 Agarwal, A., Gupta, A. C., Bachev, R., et al. 2015, *MNRAS*, **451**, 3882  
 Andruchow, I., Cellone, S. A., Romero, G. E., Dominici, T. P., & Abraham, Z. 2003, *A&A*, **409**, 857  
 Andruchow, I., Combi, J. A., Muñoz-Arjonilla, A. J., et al. 2011, *A&A*, **531**, A38  
 Bessell, M. S., Castelli, F., & Plez, B. 1998, *A&A*, **333**, 231  
 Blandford, R. D., & Rees, M. J. 1978, *PhysS*, **17**, 265  
 Brown, M. B., & Forsythe, A. B. 1974, *J. Am. Stat. Assoc.*, **69**, 364  
 Calafut, V., & Wiita, P. J. 2015, *JApA*, **36**, 255  
 Camenzind, M., & Krockenberger, M. 1992, *A&A*, **255**, 59  
 Cardelli, J. A., Clayton, G. C., & Mathis, J. S. 1989, *ApJ*, **345**, 245  
 Cellone, S. A., Romero, G. E., Combi, J. A., & Martí, J. 2007, *MNRAS*, **381**, L60  
 Chakrabarti, S. K., & Wiita, P. J. 1993, *ApJ*, **411**, 602  
 de Diego, J. A. 2010, *AJ*, **139**, 1269  
 Dey, L., Valtonen, M. J., Gopakumar, A., et al. 2018, *ApJ*, **866**, 11  
 Dickel, J. R., Yang, K. S., McVittie, G. C., & Swenson, G. W., Jr. 1967, *AJ*, **72**, 757  
 Fiorucci, M., & Tosti, G. 1996, *A&AS*, **116**, 403  
 Gaur, H., Gupta, A. C., Bachev, R., et al. 2015, *MNRAS*, **452**, 4263  
 Gaur, H., Gupta, A. C., Lachowicz, P., & Wiita, P. J. 2010, *ApJ*, **718**, 279  
 Gaur, H., Gupta, A. C., Strigachev, A., et al. 2012a, *MNRAS*, **420**, 3147  
 Gaur, H., Gupta, A. C., Strigachev, A., et al. 2012b, *MNRAS*, **425**, 3002  
 Gaur, H., Gupta, A. C., & Wiita, P. J. 2012c, *AJ*, **143**, 23  
 Gaur, H., Gupta, A. C., Wiita, P. J., et al. 2014, *ApJL*, **781**, L4  
 Ghisellini, G., Villata, M., Raiteri, C. M., et al. 1997, *A&A*, **327**, 61  
 Giannios, D., Uzdensky, D. A., & Begelman, M. C. 2009, *MNRAS*, **395**, L29  
 Gopal-Krishna, Stalin, C. S., Sagar, R., & Wiita, P. J. 2003, *ApJL*, **586**, L25  
 Gopal-Krishna, & Wiita, P. J. 1992, *A&A*, **259**, 109  
 Goyal, A., Gopal-Krishna, Wiita, P. J., et al. 2012, *A&A*, **544**, A37  
 Graff, P. B., Georganopoulos, M., Perlman, E. S., & Kazanas, D. 2008, *ApJ*, **689**, 68  
 Gu, M. F., Lee, C.-U., Pak, S., Yim, H. S., & Fletcher, A. B. 2006, *A&A*, **450**, 39  
 Gupta, A. C., Agarwal, A., Bhagwan, J., et al. 2016, *MNRAS*, **458**, 1127  
 Gupta, A. C., Agarwal, A., Mishra, A., et al. 2017a, *MNRAS*, **465**, 4423  
 Gupta, A. C., Banerjee, D. P. K., Ashok, N. M., & Joshi, U. C. 2004, *A&A*, **422**, 505  
 Gupta, A. C., Fan, J. H., Bai, J. M., & Wagner, S. J. 2008, *AJ*, **135**, 1384  
 Gupta, A. C., Krichbaum, T. P., Wiita, P. J., et al. 2012, *MNRAS*, **425**, 1357  
 Gupta, A. C., Mangalam, A., Wiita, P. J., et al. 2017b, *MNRAS*, **472**, 788  
 Hagen-Thorn, V. A., Larionov, V. M., Jorstad, S. G., et al. 2008, *ApJ*, **672**, 40  
 Heidt, J., & Wagner, S. J. 1996, *A&A*, **305**, 42  
 Hu, S.-M., Han, S.-H., Guo, D.-F., & Du, J.-J. 2014, *RAA*, **14**, 719  
 Hughes, P. A., Aller, H. D., & Aller, M. F. 1985, *ApJ*, **298**, 301  
 Joshi, M., & Böttcher, M. 2011, *ApJ*, **727**, 21  
 Kirk, J. G., Rieger, F. M., & Mastichiadis, A. 1998, *A&A*, **333**, 452  
 Kushwaha, P., Gupta, A. C., Wiita, P. J., et al. 2018a, *MNRAS*, **473**, 1145  
 Kushwaha, P., Gupta, A. C., Wiita, P. J., et al. 2018b, *MNRAS*, **479**, 1672  
 Kushwaha, P., Sahayanathan, S., & Singh, K. P. 2013, *MNRAS*, **433**, 2380  
 Larionov, V. M., Jorstad, S. G., Marscher, A. P., et al. 2008, *A&A*, **492**, 389  
 Larionov, V. M., Jorstad, S. G., Marscher, A. P., et al. 2013, *ApJ*, **768**, 40  
 Larionov, V. M., Villata, M., Raiteri, C. M., et al. 2016, *MNRAS*, **461**, 3047  
 Lehto, H. J., & Valtonen, M. J. 1996, *ApJ*, **460**, 207  
 Mangalam, A. V., & Wiita, P. J. 1993, *ApJ*, **406**, 420  
 Marcha, M. J. M., Browne, I. W. A., Impey, C. D., & Smith, P. S. 1996, *MNRAS*, **281**, 425  
 Marscher, A. P. 1996, in ASP Conf. Ser. 110, Blazar Continuum Variability 110, ed. H. R. Miller, J. R. Webb, & J. C. Noble (San Francisco, CA: ASP), 248  
 Marscher, A. P. 2014, *ApJ*, **780**, 87  
 Marscher, A. P., & Gear, W. K. 1985, *ApJ*, **298**, 114  
 Marscher, A. P., Gear, W. K., & Travis, J. P. 1992, in Variability of Blazars, Proc. Conf. in honor of the 100th Anniversary of the Birth of Yrjö Väisälä, ed. E. Valtaoja & M. Valtonen (Cambridge: Cambridge Univ. Press), 85  
 Marscher, A. P., Jorstad, S. G., D’Arcangelo, F. D., et al. 2008, *Natur*, **452**, 966  
 Miller, H. R., Carini, M. T., & Goodrich, B. D. 1989, *Natur*, **337**, 627  
 Moore, R. L., Angel, J. R. P., Duerr, R., et al. 1982, *ApJ*, **260**, 415  
 Nilsson, K., Takalo, L. O., Lehto, H. J., & Sillanpää, A. 2010, *A&A*, **516**, A60  
 O’Brien, S. 2017, arXiv:1708.02160  
 O’Riordan, M., Pe’er, A., & McKinney, J. C. 2017, *ApJ*, **843**, 81  
 Pollack, M., Pauls, D., & Wiita, P. J. 2016, *ApJ*, **820**, 12  
 Pursimo, T., Takalo, L. O., Sillanpää, A., et al. 2000, *A&AS*, **146**, 141  
 Sillanpää, A., Haerala, S., Valtonen, M. J., Sundelius, B., & Byrd, G. G. 1988, *ApJ*, **325**, 628  
 Sillanpää, A., Takalo, L. O., Pursimo, T., et al. 1996a, *A&A*, **305**, L17  
 Sillanpää, A., Takalo, L. O., Pursimo, T., et al. 1996b, *A&A*, **315**, L13  
 Smith, P. S., Montiel, E., Rightley, S., et al. 2009, arXiv:0912.3621  
 Spada, M., Ghisellini, G., Lazzati, D., & Celotti, A. 2001, *MNRAS*, **325**, 1559  
 Stalin, C. S., Gopal Krishna, Sagar, R., & Wiita, P. J. 2004, *JApA*, **25**, 1  
 Stocke, J. T., Morris, S. L., Gioia, I. M., et al. 1991, *ApJS*, **76**, 813  
 Valtonen, M., Kidger, M., Lehto, H., & Poyner, G. 2008a, *A&A*, **477**, 407  
 Valtonen, M., Zola, S., Jermak, H., et al. 2017, *Galax*, **5**, 83  
 Valtonen, M. J., Lehto, H. J., Nilsson, K., et al. 2008b, *Natur*, **452**, 851  
 Valtonen, M. J., Mikkola, S., Merritt, D., et al. 2010, *ApJ*, **709**, 725  
 Valtonen, M. J., Nilsson, K., Villforth, C., et al. 2009, *ApJ*, **698**, 781  
 Valtonen, M. J., Zola, S., Ciprini, S., et al. 2016, *ApJL*, **819**, L37  
 Villforth, C., Nilsson, K., Heidt, J., et al. 2010, *MNRAS*, **402**, 2087  
 Wagner, S. J., & Witzel, A. 1995, *ARA&A*, **33**, 163  
 Wierzholska, A., Ostrowski, M., Stawarz, L., Wagner, S., & Hauser, M. 2015, *A&A*, **573**, A69  
 Woo, J.-H., & Urry, C. M. 2002, *ApJ*, **579**, 530